Reanalysis of NOAA H_2 observations: implications for the H_2 budget

Fabien Paulot[1], Gabrielle Pétron[2,3], Andrew M. Crotwell[2,3], and Matteo B. Bertagni[4,5]

[1]Geophysical Fluid Dynamics Laboratory, National Oceanic and Atmospheric Administration, Princeton, NJ, USA
[2]Cooperative Institute for Research in Environmental Sciences, University of Colorado Boulder, Boulder, CO, USA
[3]Global Monitoring Laboratory, National Oceanic and Atmospheric Administration, Boulder, CO, USA
[4]High Meadow Environmental Institute, Princeton University, Princeton, NJ, USA
[5]Department of Civil and Environmental Engineering, Princeton University, Princeton, NJ, USA

Correspondence: Fabien Paulot (fabien.paulot@noaa.gov)

Abstract. Hydrogen (H_2) is a promising low-carbon alternative to fossil fuels for many applications. However, significant gaps in our understanding of the atmospheric H_2 budget limit our ability to predict the impacts of greater H_2 usage. Here we use NOAA H_2 dry air mole fraction observations from air samples collected from ground-based and ship platforms from 2010 to 2019 to evaluate the representation of H_2 in the NOAA GFDL-AM4.1 atmospheric chemistry-climate model. We find that the base model configuration captures the observed interhemispheric gradient well but underestimates the surface concentration of H_2 by about 10 ppb. Additionally, the model fails to reproduce the 1-2 ppb/year mean increase in surface H_2 observed at background stations. We show that the cause is likely an underestimation of current anthropogenic emissions, including potential leakages from H_2-producing facilities. We also show that changes in soil moisture, soil temperature, and snow cover have likely caused an increase in the magnitude of the soil sink, the most important removal mechanism for atmospheric H_2, especially in the Northern Hemisphere. However, there remains uncertainty due to fundamental gaps in our understanding of H_2 soil removal, such as the minimum moisture required for H_2 soil uptake, for which we performed extensive sensitivity analyses. Finally, we show that the observed meridional gradient of the H_2 mixing ratio and its seasonality can provide important constraints to test and refine parameterizations of the H_2 soil sink.

1 Introduction

Increased hydrogen (H_2) usage has been proposed as a strategy to reduce the carbon intensity of many sectors of the economy that are difficult to electrify (Hydrogen Council, 2017; da Silva Veras et al., 2017; Staffell et al., 2019; Abe et al., 2019; Dawood et al., 2020). The climate benefits of greater H_2 usage depend primarily on the H_2 production pathway. Current H_2 production is dominated by steam reforming of methane (CH_4) in natural gas (Holladay et al., 2009; International Energy Agency, 2019), a process that is very carbon intensive (Howarth and Jacobson, 2021). Carbon capture can reduce CO_2 emissions associated with H_2 production. However, methane leakage throughout the supply chain could offset much of the expected climate benefits of increased H_2 usage (Howarth and Jacobson, 2021; Ocko and Hamburg, 2022; Bertagni et al., 2022; Hauglustaine et al., 2022). Alternative production pathways such as renewable-based electrolytic H_2 can provide large and rapid reductions in radiative

forcing (Hauglustaine et al., 2022), and considerable investments have been devoted to reducing their cost (International Energy Agency, 2022). Furthermore, evidence of significant concentrations of H_2 in surface and subsurface natural gases (Zgonnik, 2020; Milkov, 2022; Lefeuvre et al., 2021) have spurred interest in the potential of naturally occurring H_2 as a new primary energy source (Prinzhofer et al., 2018; Lapi et al., 2022).

H_2 photooxidation in the atmosphere also tends to increase CH_4, O_3, and stratospheric water vapor, which results in indirect radiative forcing (Derwent et al., 2001; Paulot et al., 2021). Sand et al. (2023) recently calculated that H_2 has a global warming potential of $\simeq 11.6 \pm 2.8$ and 37.3±15.1 for a 100 and 20-year time horizon, respectively.

Significant uncertainties regarding the overall budget of H_2 remain. H_2 sources include both emissions and photochemical production from the oxidation of volatile organic compounds (VOCs). Estimates for the overall source of atmospheric H_2 range from $\simeq$ 70 to 110 Tg/yr, a large spread primarily associated with the magnitude of the H_2 photochemical sources (Ehhalt and Rohrer, 2009). Recent work also argues that current estimates of H_2 sources need to be revised upward to account for geologic H_2 seepage (Zgonnik, 2020). These uncertainties in the nature and magnitude of H_2 sources have proved challenging to reduce in part because of commensurate uncertainties in H_2 sinks. The atmospheric oxidation of H_2 by OH is well understood but is estimated to account for less than one third of the overall atmospheric sink (Ehhalt and Rohrer, 2009; Paulot et al., 2021). The most important removal pathway is the consumption of H_2 by high-affinity hydrogen oxidizing bacteria (HA-HOB), a class of bacteria that have been identified in many different soils (Constant et al., 2008; Greening et al., 2015; Bay et al., 2021; Greening and Grinter, 2022). Several parameterizations of the H_2 soil sink have been developed (Ehhalt and Rohrer, 2013; Price et al., 2007; Smith-Downey et al., 2006; Bertagni et al., 2021) that aim at capturing the observed sensitivity of H_2 soil removal to soil temperature, soil moisture and ecosystem/soil type (Ehhalt and Rohrer, 2009). However, observational constraints on H_2 soil removal remain very limited (Meredith et al., 2016) and this process remains challenging to represent in global models (Yashiro et al., 2011; Paulot et al., 2021).

Here, we leverage the recently completed recalibration of H_2 measurements collected by NOAA Global Monitoring Laboratory to perform a comprehensive evaluation of the simulation of H_2 in the Geophysical Dynamics Laboratory (GFDL) AM4.1 model (Horowitz et al., 2020; Paulot et al., 2021). The NOAA monitoring network provides additional spatial coverage that complements other existing networks (AGAGE (Prinn et al., 2018), CSIRO (Francey et al., 2003)) and offers a unique opportunity to evaluate the skill of the model in capturing changes in H_2 atmospheric concentration since 2010. This period is especially important to gain a quantitative understanding of the present-day H_2 budget, also given that recent H_2 observations at Mace Head (Derwent et al., 2021, 2023) show both an increase in H_2 concentration and its soil removal rate. The study is organized as follows: we first describe and evaluate the representation of H_2 in the GFDL-AM4.1 global chemistry-climate model, focusing on changes in H_2 over the 2010–2019 period. We then assess the sensitivity of the H_2 simulations to uncertainties in the H_2 budget focusing on the representation of anthropogenic H_2 emissions and soil removal.

2 Methods

2.1 Observations

NOAA Global Monitoring Laboratory (GML) provides long-term monitoring of long-lived greenhouse gases and other trace species. The NOAA GML Global Cooperative Air Sampling Network is a partnership between GML and many outside organizations and individual volunteers to collect discrete air samples approximately weekly from 60+ globally distributed sites (Global Monitoring Laboratory, 2023). These sites are often situated to collect air representative of large regional air masses. Priorities are placed on sites where opportunities exist for local support which can be maintained over long (decadal) time scales. The discrete air samples are collected weekly in pairs of 2 L glass flasks and are returned to GML for measurements of multiple species on central measurement systems thus providing a high level of consistency across the globally distributed network.

GML measurements of H_2 in the discrete air samples began in the late 1980's as an opportunistic measurement associated with the analytical technique then used for measuring atmospheric carbon monoxide (CO). To facilitate these H_2 measurements, NOAA/GML developed an in-house H_2-in-air reference scale based on a few gravimetric standards (the latest iteration named H2-X1996). This reference scale was not stable over time and introduced significant time-dependent measurement errors. GML recently converted part of the historical H_2 measurement records to the H_2 calibration scale recommended by the World Meteorological Organization (WMO/MPI H2-X2009) maintained by Max Planck Institute (MPI) in Jena, Germany (Jordan and Steinberg, 2011). Measurements since approximately 2010 have been reprocessed onto the MPI scale to remove the biases inherent in the NOAA X1996 scale (Pétron et al., in review, 2024). NOAA reprocessed H_2 data since 2010 is consistent to within 1-2 ppbv on an annual basis for same air measurements with CSIRO and the MPI-BGC (Pétron et al., in review, 2024). However, earlier NOAA data that remains on the obsolete NOAA X1996 scale is known to be biased relative to the later NOAA data and to other monitoring programs.

Here, we only consider ground stations from the NOAA cooperative air sampling network with at least 96 distinct monthly observations over the 2010-2019 period (80% coverage, Fig. S1). Ship-based observations are binned in 4°x4° regions and we only consider regions with at least 40 observations.

2.2 Model setup

We use the GFDL Atmospheric Chemistry Model AM4.1 (Horowitz et al., 2020). For all configurations, the model is run from 2004 to 2019. Monthly sea surface temperature and sea ice concentration are from Rayner et al. (2003) and Taylor et al. (2000). Horizontal winds are nudged to 6-hourly horizontal winds from the National Center for Environmental Prediction (Kalnay et al., 1996). The model output is sampled at the time and location of the air sampling. To better quantify the drivers of the H_2 distribution and trend, we tag H_2 associated with anthropogenic, marine, soil, and biomass burning direct H_2 emissions and H_2 produced by the oxidation of VOCs.

2.2.1 BASE simulation

AM4.1 includes a detailed representation of H_2 (Paulot et al., 2021), which is briefly summarized here. This configuration will be referred to as BASE (Table 1), hereafter. H_2 sources include both direct emission from anthropogenic and natural sources as well as photochemical production. Anthropogenic emissions of H_2 ($\simeq$ 13 Tg/yr over the 2010–2019 period) are estimated from CO emissions in the Community Emissions Data System (CEDS) v20210421 (O'Rourke et al., 2021) using time-invariant sector–specific emission H_2:CO emissions ratios (Table S1). The transportation and residential sectors are the largest contributors to anthropogenic H_2 emissions (Fig. S2). Biomass burning emissions ($\simeq$ 8 Tg/yr) are estimated using the Global Fire Emissions Database (GFED4s, van der Werf et al. (2017)) with emission factors from Akagi et al. (2011) and Andreae (2019). Marine (6 Tg/yr) and terrestrial (3 Tg/yr) sources of H_2 are prescribed as a monthly climatology and distributed spatially (Fig. S3) based on the soil and marine CO emission patterns in the Precursors of Ozone and their Effects in the Troposphere inventory (Granier et al., 2005). The BASE emission inventory does not include geological sources of H_2.

The production of H_2 associated with CH_2O photolysis is calculated interactively using FAST-JX version 7.1, as described by Li et al. (2016). Formaldehyde sources are dominated by the oxidation of VOCs from anthropogenic (O'Rourke et al., 2021), biomass burning (van der Werf et al., 2017), and natural origins. Biogenic emissions of VOCs are prescribed as a monthly climatology (Granier et al., 2005), except for isoprene and terpenes, of which emissions are calculated interactively using the Model of Emissions of Gases and Aerosols from Nature (Guenther et al., 2012). Surface CH_4 is prescribed as a monthly latitudinal profile from observations up to 2014 (Meinshausen et al., 2017) and from the SSP1-2.6 scenario after 2015 (Meinshausen et al., 2020). We select this scenario as it tracks well the observed global CH_4 surface mixing ratio from the World Meteorological Organization Global Atmospheric Watch greenhouse gases observational network (WMO, 2021). To characterize the contribution of different VOC emissions to the photochemical production of H_2, we perform a set of sensitivity experiments in which we perturb the emission of a given VOC by 10% and quantify the response of H_2 production. For CH_4 oxidation, we directly track the different oxidation pathways that result in H_2 production. The molar yield of H_2 from CH_4, isoprene, methanol, and terpene are estimated to be 0.38, 0.56, 0.21, and 0.70 mol/mol, respectively. These yields are broadly similar to estimates derived by Ehhalt and Rohrer (2009) (0.37, 0.54, 0.19, 0.71, respectively) but are lower than estimates derived from box-model (0.38, 0.83, 0.38, and 0.85, respectively for NO_x=160 pptv (Grant et al., 2010)), which may reflect the impact of wet and dry deposition. In particular, Fig. S4 shows that the simulated yield of H_2 from CH_4 oxidation is lowest in the tropics, where most CH_4 is oxidized, as a greater fraction of CH_2O is oxidized by OH in this region than at high latitudes.

Overall, we find that CH_4 oxidation is the largest photochemical source of H_2 ($\simeq$27 Tg/yr). The oxidation of biogenic VOCs (BVOCs) accounts for the majority of the remaining photochemical source of H_2 ($\simeq 14$ Tg/yr) primarily from isoprene (8 Tg/yr), methanol (3 Tg/yr), and terpene (1.5 Tg/yr). The oxidation of VOCs from anthropogenic and biomass burning origin produces $\simeq$3 Tg/yr of H_2. Our estimates are in good agreement with previous estimates (Ehhalt and Rohrer, 2009): CH_4 (23 ± 8 Tg/yr), isoprene (9 ± 6 Tg/yr), biomass burning and anthropogenic VOCs (3 Tg/yr). This similarity can attributed to the similar yield of H_2 from CH_2O (0.4 mol/mol compared to 0.37 (Ehhalt and Rohrer, 2009)). More work is needed to better characterize the temperature and pressure sensitivity of CH_2O photolysis quantum yields (Röth and Ehhalt, 2015).

Fig. 1a summarizes the simulated sources of H_2 associated with photochemical production and direct emissions in the BASE run. Over the 2010-2019 period, the average global simulated source of H_2 is 74±1 Tg/yr, with 60% from photochemical production. Anthropogenic activities are estimated to account for $\simeq$ 40% of the overall H_2, primarily from the CH_4 oxidation. Note that we assume that 50% of the photochemical production of H_2 from CH_4 oxidation is anthropogenic based on the detailed bottom-up inventory of CH_4 sources (Saunois et al., 2020). Top-down estimates suggest a higher contribution of anthropogenic sources ($\simeq 60\%$, Saunois et al. (2020)), which would further increase the fraction of H_2 associated with anthropogenic activities. Fig. 1b shows that the simulated total source of H_2 changes little over the 2010–2019 period. The simulated annual photochemical source of H_2 (excluding non-methane VOCs from biomass burning and anthropogenic origins) is 1.6 Tg/yr greater in 2017-2019 than in 2010-2012, with 70% of this increase attributed to CH_4. In contrast, H_2 associated with anthropogenic activities decreases (-1.3 Tg/yr, Fig. S2a), mostly from transport (-1 Tg/yr) and industries (-0.4 Tg/yr). The decrease in H_2 emissions reflects the decline in CO emissions from these sectors. The interannual variability of the overall H_2 source over the 2010-2019 period is dominated by the variability of biomass burning emissions, which can result in interannual changes of $\simeq 2$ Tg/yr.

H_2 sinks include chemical oxidation by OH and O(^{1}D), and soil uptake associated with microbial activity. The deposition velocity of H_2 ($v_d(H_2)$) over land is calculated following the parameterization of Ehhalt and Rohrer (2013) and depends on temperature, soil moisture (Ehhalt and Rohrer, 2013) and soil carbon (Khdhiri et al., 2015; Paulot et al., 2021). In the BASE configuration we use a monthly climatology of $v_d(H_2)$ calculated using monthly meteorological and soil outputs from the GFDL Earth System Model ESM4.1 over the 1989–2014 period (Dunne et al., 2020; Paulot et al., 2021). Soil uptake is estimated to account for 71% of the overall H_2 sink. The overall lifetime of H_2 in the BASE configuration is 2.5 years. The lifetime of H_2 associated with anthropogenic emissions is 6% shorter due to their geographical distribution.

2.2.2 Sensitivity simulations

In this section, we describe additional model simulations that are designed to explore the impact of uncertainties in the representation of H_2 emission and deposition on the simulation of atmospheric H_2 (Table 1). We focus on H_2 emissions and deposition as their representations in models are largely derived from limited observational constraints (Derwent et al., 2023; Paulot et al., 2021).

The REVISED configuration focuses on the representation of anthropogenic and natural H_2 emissions. The development of the REVISED emission inventory is guided by the biases of the BASE configuration against H_2 observations (Supporting materials S1.1, Ghosh et al. (2015)). In particular, we focus on the representation of transportation emissions (Table S1) and emissions associated with industrial H_2 use for refining, ammonia, methanol and steel production. Further details regarding the treatment of anthropogenic and natural sources in the REVISED emission inventory can be found in the Supporting materials (Texts S1.2 and S1.3)

We further consider the impact of a different representation of H_2 soil uptake on the simulation of H_2. Here, we use the parameterization of the soil moisture response of HA-HOB activity recently developed by Bertagni et al. (2021). This parameterization relates the minimum soil moisture required for H_2 uptake by HA-HOB to soil hydrological properties, which

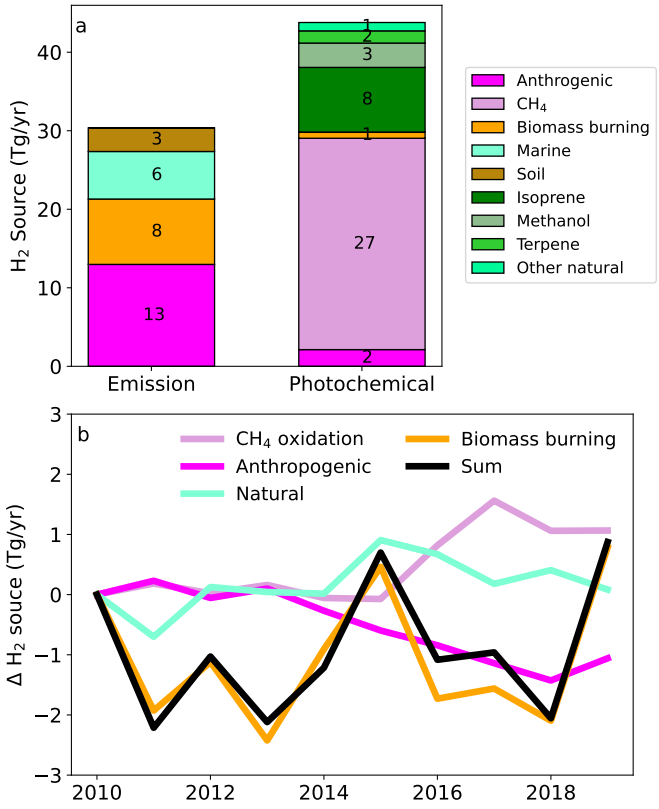

Figure 1. Global source of H_2 (panel a). Panel b shows the changes in the magnitude of H_2 sources over the 2010–2019 period. For clarity, the green line denotes the combined change in H_2 emissions and photochemical production from natural sources (marine and soil emissions + BVOCs photooxidation).

facilitates its incorporation in global models. This model also allows to vary the strength of the diffusion barrier associated with soil litter, which can reduce H_2 transport to active sites (Smith-Downey et al., 2008; Ehhalt and Rohrer, 2009). To quantify possible changes in $v_d(H_2)$ over the 2010-2019 period, we calculate daily deposition velocity using 3-hourly soil moisture, soil temperature, and snow cover from the NASA Global Land Data Assimilation System (Rodell et al., 2004). We focus on two different configurations. In REVISED_GLDAS, we neglect the litter resistance and assume that HA-HOB activity is inhibited when the soil matrix potential (Ψ_{ws}) is less than the wilting point of plants in semiarid environments ($\Psi_{ws} = -3000$ kPa) as recommended by Bertagni et al. (2021). The required soil moisture for the H_2 uptake is not well known and experimental studies have shown that HA-HOB are present in very arid environments (Jordaan et al., 2020). In REVISED_GLDAS2, we assume a much lower activation threshold for HA-HOB ($\Psi_{ws} = -10,000$ kPa) and account for the litter barrier. Note that both these configurations use the REVISED emission inventory. More details regarding the calculation of $v_d(H_2)$ can be found in the Supporting materials (Text S1.4).

Table 1. Model configurations

	H_2 anthropogenic emission	H_2 natural emission	H_2 soil removal
BASE	Time-invariant H_2:CO emission ratio (Table S1)	Ocean+Soil: Monthly climatology Biomass burning: GFED4s	Monthly climatology $v_d(H_2)$ (Paulot et al., 2021)
REVISED	Revised H_2:CO emission ratio Emission from industrial H_2 use (Text S1.2 and Table S1)	Ocean: Calculated from CO seawater concentration Soil: Calculated from N fixation (Text S1.3) Biomass burning: same as BASE	Same as BASE
REVISED_GLDAS	same as REVISED	Same as REVISED	Daily $v_d(H_2)$ calculated using land reanalysis with soil moisture sensitivity from Bertagni et al. (2021) (Text S1.4)
REVISED_GLDAS2	same as REVISED	Same as REVISED	Same as REVISED_GLDAS with canopy+litter resistance and a lower HA-HOB water-activation threshold (Text S1.4)

3 Results and discussion

3.1 BASE model evaluation

3.1.1 Climatology

Fig. 2 shows the average model bias against surface observations from NOAA GML. In the BASE configuration, AM4.1 underestimates H_2 at all stations, with greater biases over continental regions (Fig. 2). Correlations exceed 0.5 at more than 90% of background sites (square) but only at 55% of continental sites. Fig. 2b further shows that the concentration at the South pole is $\simeq$ 50 ppb greater than at the North pole, which is well captured by the BASE configuration.

To examine differences between the model and observed seasonality, we first apply the Kmean++ clustering algorithm (Arthur and Vassilvitskii, 2007) to the observed H_2 monthly climatology. Since our focus is on the seasonality of H_2 we transform the monthly climatology of H_2 at each site such that it has a mean of 0 and a standard deviation of 1. Using the within-cluster sum of squares and the silhouette score, we find that the standardized H_2 observations can be well represented using 4 clusters. Fig. 3 shows the seasonality of the standardized H_2 concentration for each cluster (panel a) as well as their spatial distribution (panel b). Sites are found to cluster broadly by latitude based on the seasonality of H_2 with clusters 1, 2, 3, and 4 being comprised primarily of sites located in the Southern mid to high latitudes, Southern tropics, Northern subtropics, and Northern mid to high latitudes, respectively. The model captures the seasonality of H_2 well in the Southern Hemisphere (cluster 1) but peaks 1 to 3 months earlier than observations for clusters 2, 3 and 4. Fig. 3c shows the contribution of different

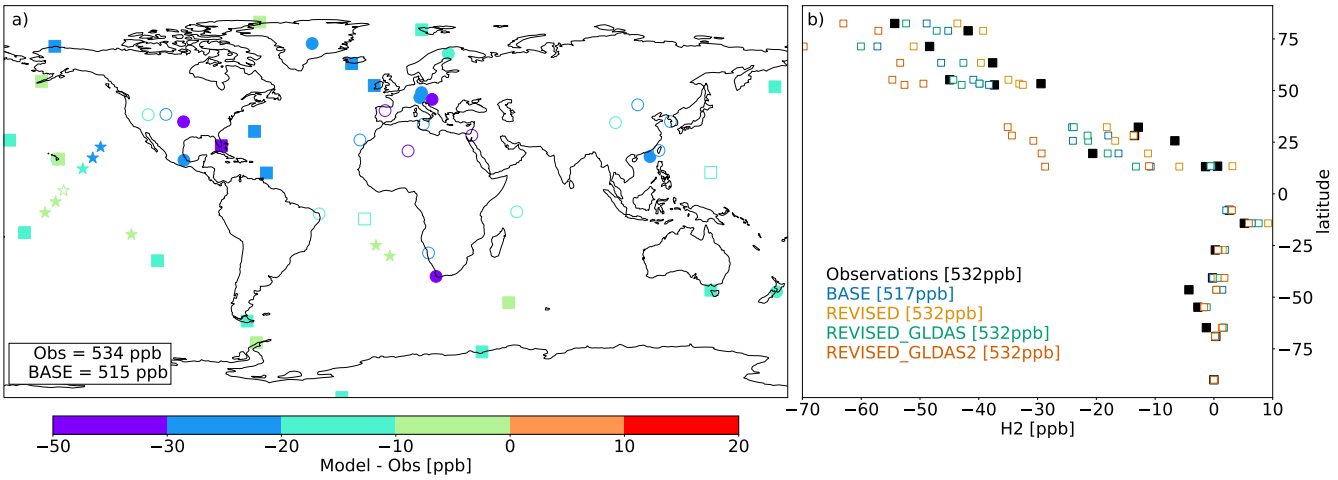

Figure 2. Mean model bias at individual sites for the BASE model configuration (a) over the 2010–2019 period. Filled symbols denote sites where the correlation between observed and simulated H_2 concentrations exceeds 0.5. Square and star symbols denote background sites and cruises, respectively. Panel (b) shows the observed and simulated difference in H_2 at background sites relative to H_2 mole fraction measured at the South Pole observatory. The average concentrations at background sites is indicated for each configuration in the legend.

sources of H_2 to the simulated seasonality of H_2 (inferred from the tagged H_2 tracers). The seasonal bias for cluster 2 is primarily driven by H_2 emitted from biomass burning, which peaks $\sim$ 2 months earlier than observations. This delay may be associated with greater burning of woody material towards the end of the dry season, emitting more incompletely oxidized products such as H_2 (van der Werf et al., 2006). Fig. 3c also shows that the seasonal bias in clusters 3 and 4 may be associated with H_2 emitted by anthropogenic activities. As we will show in section 3.2.2, this seasonal bias may also reflect errors in the removal of H_2.

3.1.2 Time series

Fig. 4 shows that H_2 has increased at most sites with an average trend at background sites of 1.4$\pm$0.7 ppb/yr over the 2010-2019 period with little variability with latitude. Trends are calculated using ordinary least-square regression applied to the deseasonalized monthly H_2 concentrations. In contrast, simulated H_2 concentration in the BASE configuration changes little over this time period.

In the Northern hemisphere, the lack of trend at background sites in the model (Fig. 4c) reflects the near-cancellation between the increase of photochemically-produced H_2 and the decrease of H_2 emitted from anthropogenic sources, consistent with the changes in anthropogenic emissions and the photochemical source of H_2 from CH_4 and biogenic VOCs oxidation (Fig. 1). The simulated absolute trend in anthropogenic hydrogen is $\simeq$ 50% lower in the Southern Hemisphere relative to the Northern Hemisphere due to the higher relative areal density of anthropogenic sources in the Northern Hemisphere. In contrast, the change in photochemically-produced H_2 exhibits little variability with latitude and matches the observed trend

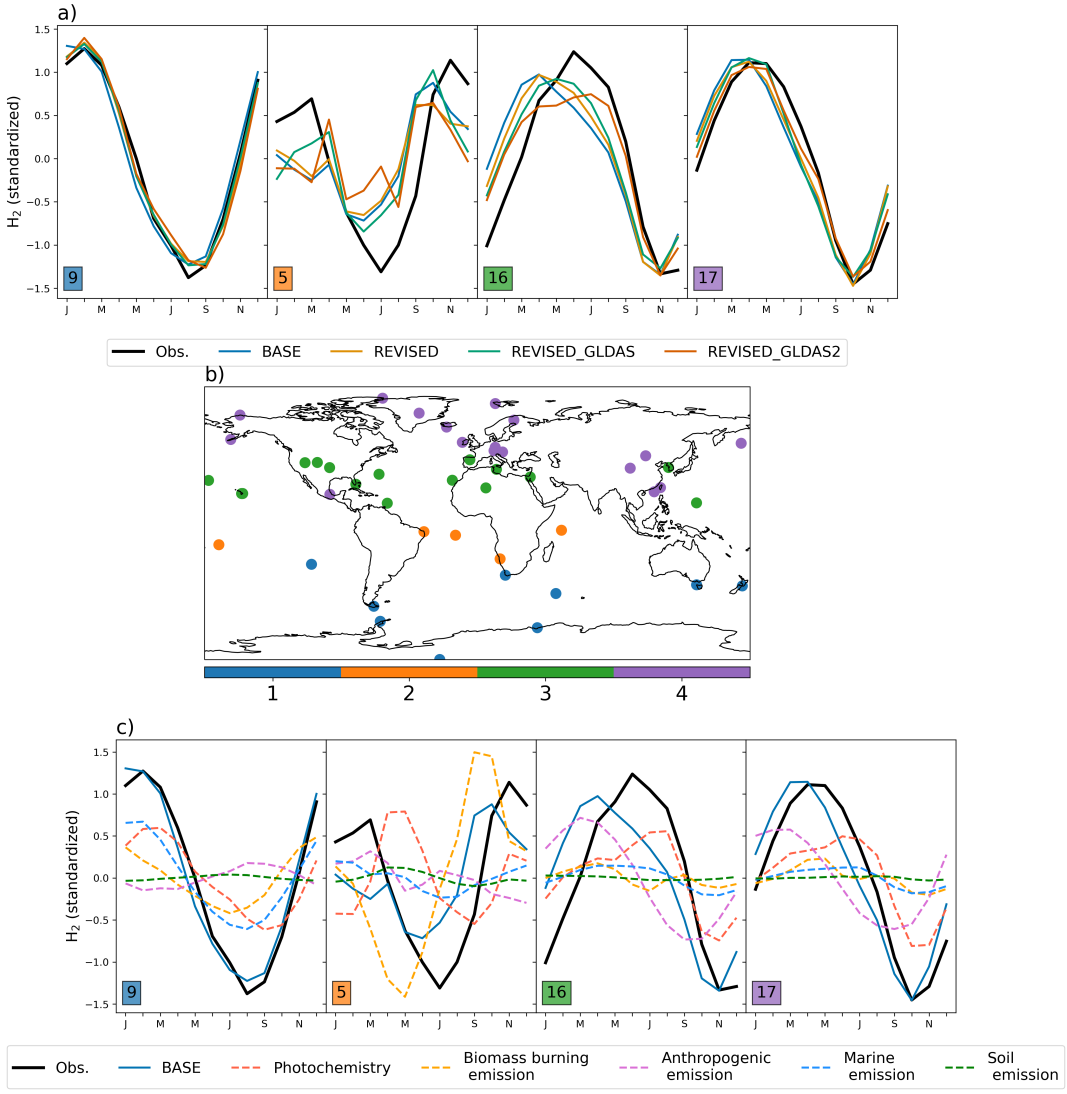

Figure 3. Monthly standardized H_2 concentration for each cluster (a). The number of sites in each cluster is indicated by insets. The sites included in each cluster are shown in panel (b). The variation of source-tagged H_2 tracers in each cluster is shown in panel (c). Source-tagged H_2 tracers are normalized using the standard deviation of simulated H_2.

well. The simulated trend also shows little latitudinal variation due to a decrease in H_2 from biomass burning in the Southern Hemisphere.

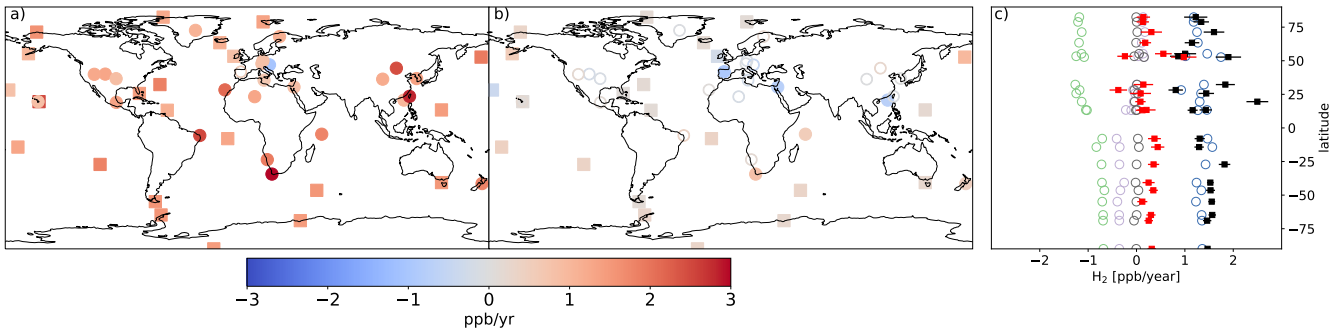

Figure 4. Trend in H_2 concentrations in observations (a) and in the BASE simulation (b) over the 2010–2019 period. Panel (c) shows the observed (black) and simulated (red) trend in H_2 at background sites (squares) as well as the trend in tagged H_2 tracers associated with anthropogenic sources (green), biomass burning (purple), ocean+soil sources (black), and photochemical production (blue). Filled symbols denote trends that are significantly different from 0 ($p<0.01$). The error bars show one standard deviation for the estimated observed and simulated trends.

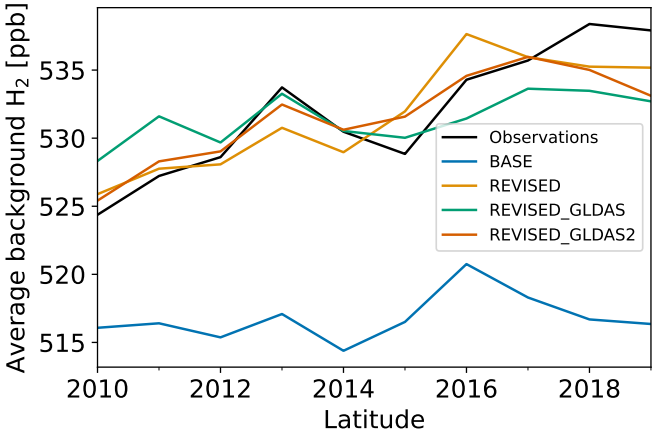

Figure 5. Mean observed and simulated H_2 at background sites (see Fig. 2 for locations)

3.2 Sensitivity simulations

In this section, we explore how uncertainties in the representation of H_2 emissions and deposition contribute to the biases in the BASE model run.

3.2.1 Emission

Fig. 5 shows that the BASE run exhibits a 10-15 ppb negative bias and fails to capture the $\simeq$ 15 ppb increase over the 2010–2019 period (Fig. 5). From this bias, we estimate a missing source of H_2 of $\simeq$ 2-2.5 Tg/yr circa 2010 and 3-4 Tg/yr circa

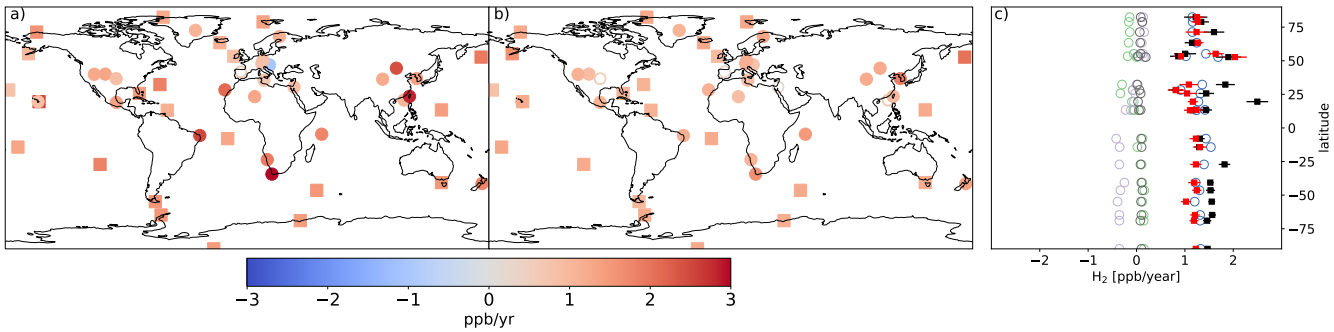

Figure 6. Same as Fig. 4 but for the REVISED configuration

2019 (Text S1.1). Similarly, Derwent et al. (2023) recently reported that a missing H_2 source (5 Tg/yr in 2020) was required to explain the observed increase in H_2 concentration at Mace Head and Cape Grim since 2010.

Figs 5 and 6 show that the observed increase in H_2 can be well captured with the REVISED emission inventory. In this inventory, the increase in the missing source of H_2 is explained by a lower decrease in anthropogenic H_2 emissions associated with fossil fuel combustion (0.9 Tg/yr lower in 2019 relative to 2010 compared to 1.6 Tg/yr in the BASE inventory) and an increase in H_2 emissions associated with H_2 industrial usage (0.3 Tg/yr). We also increase the H_2 soil source from 3 to 4.5 Tg/yr to reduce the model negative bias. This change is well within the large uncertainties in the minor H_2 sources surveyed by Ehhalt and Rohrer (2009). In particular, it is a small fraction of the estimated geological source of H_2 (23±7 Tg/yr (Zgonnik, 2020)), which we do not account for here.

The REVISED emission inventory provides a possible explanation for the observed increase in atmospheric H_2. It highlights the importance of constraining H_2 emissions associated with H_2 industrial use, a sector that is expected to grow rapidly in coming decades.

3.2.2 Deposition

The BASE and REVISED experiments assume no interannual variability in $v_d(H_2)$. However, we have recently shown that climate change may cause an increase in $v_d(H_2)$ (Paulot et al., 2021). Recent analysis of observations at Mace Head also suggests that $v_d(H_2)$ has increased in recent decades (Derwent et al., 2021).

Fig. 7 shows that the REVISED_GLDAS and REVISED_GLDAS2 $v_d(H_2)$ exhibit different meridional distributions relative to the BASE configuration with faster removal in the subtropics and northern high latitudes but slower removal in the tropics. This reflects more efficient removal of H_2 in arid regions and slower removal in the tropics. These spatial differences are the largest for the REVISED_GLDAS2 configuration due to the activation of HA-HOB at a lower soil moisture. Fig. 7b further shows that $v_d(H_2)$ in the REVISED_GLDAS and REVISED_GLDAS2 configuration both increase over the 2010-2019 period in the Northern mid latitudes. This increase reflects drier and warmer conditions in Europe, the Western US as well as parts of Siberia, which result in faster biological uptake rates and promote H_2 diffusivity (Fig. S5). This mechanism may contribute

to the reported 1.2%/yr increase in H_2 deposition velocity at Mace Head from 1994 to 2020 (Derwent et al., 2021). Drier conditions in Australia trigger biotic limitations, which results in a large decrease in H_2 deposition velocity in the Southern mid latitudes in the REVISED_GLDAS configuration. In contrast, we find no significant suppression of H_2 uptake in Australia over this time period in the the REVISED_GLDAS2 configuration due a lower threshold for biotic limitation.

Changes to the spatial distribution of $v_d(H_2)$ and the increase in H_2 removal in the Northern mid latitudes (Fig. 7b) in REVISED_GLDAS result in a larger pole-to-pole difference in surface H_2 (Fig. 2) and a reduction in the simulated trend (Fig. 8) in the Northern mid to high latitudes. Both of these changes tend to degrade the model performance relative to the REVISED configuration. In contrast, the REVISED_GLDAS configuration better captures the timing of the H_2 maximum in the northern hemisphere (clusters 3 and 4, Fig. 3a).

Systematic assessment of the sensitivity of $v_d(H_2)$ to Ψ_{ws} and the strength of the litter barrier is shown in Fig. 9. We find that a lower soil moisture threshold for HA-HOB activation (i.e., a lower Ψ_{ws}) favors H_2 removal in the Northern hemisphere relative to the Southern hemisphere (Fig. 9a) and results in a larger increase in $v_d(H_2)$ over the 2010–2019 period (Fig. 9b), especially in the Southern hemisphere (Fig. 9c). This suggests that a lower Ψ_{ws} would tend to worsen the model performance in the absence of a litter barrier (given the REVISED emissions). The litter barrier tends to increase the importance of arid regions for H_2 removal. This makes H_2 uptake more susceptible to moisture inhibition, such that a stronger litter barrier tends to result in a lower increase of even a decrease in $v_d(H_2)$ over the 2010-2019 period. Under all scenarios, the litter barrier tends to increase the gradient in $v_d(H_2)$ between Northern and Southern hemispheres.

It is notable that no configuration results in little change in $v_d(H_2)$ without producing large and increasing gradients between the Northern and Southern hemispheres. As a result, our model cannot capture the observed trends, meridional gradient, and seasonality together given our REVISED estimate of H_2 emissions. This is illustrated by the REVISED_GLDAS2 configuration (Ψ_{ws}=-10000 kPa, Litter_scale=1), which is found to improve the simulated trend relative to the REVISED_GLDAS (not shown) and the simulated seasonality relative to the REVISED configuration (Fig. 3) but results in a large overestimate of the South/North meridional gradient (Fig. 2). This highlights the need for a more detailed representation of the factors that modulate $v_d(H_2)$ (Khdhiri et al., 2015) to help interpret changes in H_2 concentrations.

4 Conclusions

The recently released H_2 dry air mole fraction measurements from the NOAA Global Cooperative Air Sampling Network expand the spatial coverage of the WMO Global Atmospheric Watch observations. This offers the opportunity to assess the representation of the H_2 atmospheric budget in the state-of-the-art GFDL-AM4.1 global atmospheric chemistry climate model. Observations show that H_2 has increased on average by 1 to 2 ppb/year over the 2010-2019 period. This change can be explained by the increase in photochemically-produced H_2 (mostly from CH_4) provided direct anthropogenic H_2 emissions have remained stable during this time period. We hypothesize that this stability reflects the compensation between declining emissions associated with fossil fuel combustion (mostly from the transport sector) and increasing emissions associated with H_2-producing facilities (for refining, ammonia, methanol and steel production). This is notable as H_2 release from H_2 produc-

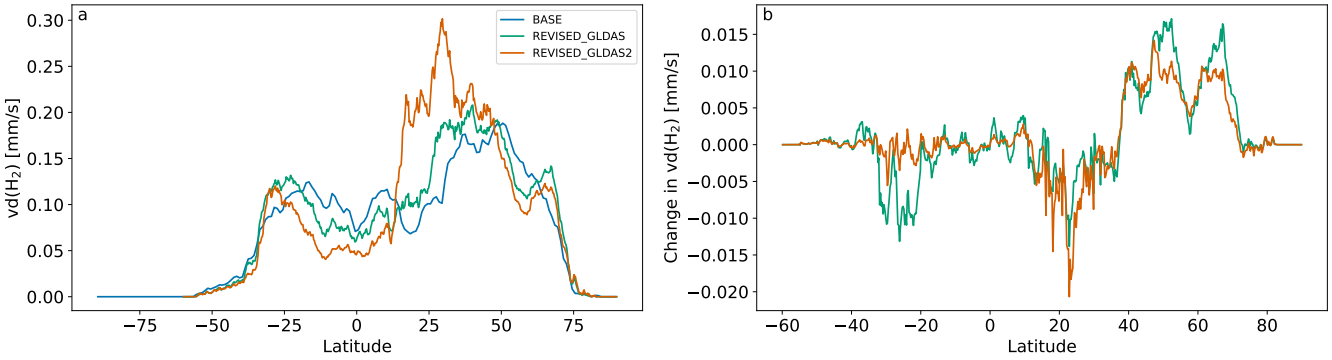

Figure 7. Meridional distribution of $v_d(H_2)$ in the BASE, REVISED_GLDAS, and REVISED_GLDAS2 simulations (a) and (b) simulated change in $v_d(H_2)$ between (2017–2019) and (2010-2012)

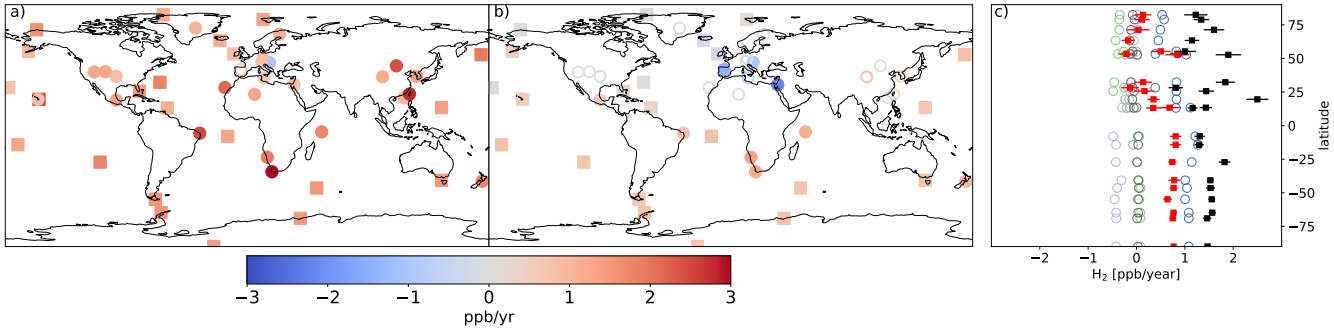

Figure 8. Same as Fig. 4 but for the REVISED_GLDAS configuration

tion facilities is poorly understood yet important to assess the climate benefits of H_2 (Hauglustaine et al., 2022; Bertagni et al., 2022).

We show that the observed trend, seasonality, and meridional gradient of H_2 provide complementary constraints on the global H_2 biogeochemical cycle. We find that our model fails to capture all three constraints together, which likely reflects fundamental gaps in our representation of the soil removal of H_2 by microorganisms (HA-HOB). Such uncertainties are important as an increase in $v_d(H_2)$ would require a commensurate increase in H_2 sources to explain the observed change in H_2 concentration.

This study highlights the need for coordinated field and laboratory data collection efforts to help improve models of the distribution and activity of HA-HOB in global models (American Academy of Microbiology, 2023). Such work is critical to quantify the response of atmospheric H_2 to increasing anthropogenic H_2 usage as well as hydrological changes associated with climate change (Jansson and Hofmockel, 2019; Huang et al., 2015) but is hindered by the lack of sensors that offer higher time resolution and maintain good sensitivity and stable response.

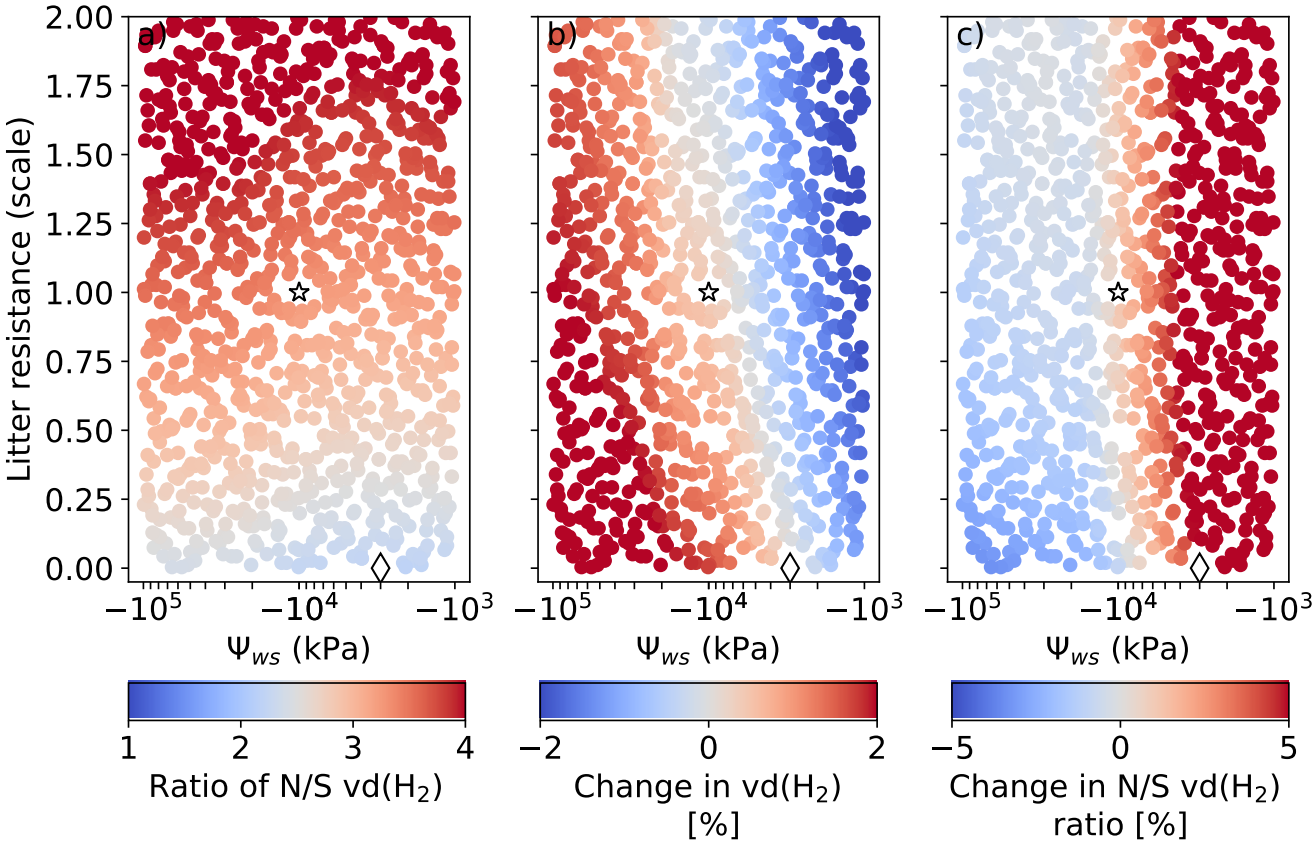

Figure 9. Simulated sensitivity of $v_d(\mathrm{H_2})$ to Ψ_{ws} and the strength of the litter diffusive barrier. Panels a, b and c show the response of the North/South ratio of $v_d(\mathrm{H_2})$, the difference in $v_d(\mathrm{H_2})$ in (2017–2019) relative to (2010-2012), and the difference in the N/S $v_d(\mathrm{H_2})$ gradient in (2017–2019) relative to (2010-2012), respectively. The REVISED_GLDAS configuration uses $\Psi_{ws} = -3000$ kPa and no litter resistance (diamond). The REVISED_GLDAS2 uses $\Psi_{ws} = -10000$ kPa and the default (scale=1) litter resistance (star). The litter scale reflects the perturbation to the default litter resistance (see Text S1.4)

Code and data availability. The code for the GFDL ESM4.1 model is available at https://zenodo.org/record/3836405. NOAA Global Cooperative Network Flask Air H_2 (Pétron et al., 2023) can be downloaded at https://doi.org/10.15138/WP0W-EZ08.

Author contributions. FP designed the research, developed, and analyzed the model simulations. GP and AC collected and processed H_2 observations from the NOAA network and provided guidance regarding their interpretation. MB developed the soil moisture parameterization of HA-HOB used in the REVISED_GLDAS and REVISED_GLDAS2 configurations. All authors contributed to the drafting of the manuscript.

Competing interests. The authors declare that they have no conflict of interest

Acknowledgements. We thank Vaishali Naik for her help with generating model-ready H_2 emissions. We thank Larry Horowitz, Vaishali Naik, Amilcare Porporato, and Xinning Zhang for their helpful comments on the manuscript. This research was supported in part by NOAA cooperative agreements NA17OAR4320101 and NA22OAR4320151 and by the U.S. Department of Energy, Office of Energy Efficiency and Renewable Energy (EERE), specifically the Hydrogen and Fuel Cell Technologies Office. The views expressed herein do not necessarily represent the views of the U.S. Department of Energy or the United States Government.

References

Abe, J., Popoola, A., Ajenifuja, E., and Popoola, O.: Hydrogen energy, economy and storage: Review and recommendation, International Journal of Hydrogen Energy, 44, 15 072–15 086, https://doi.org/10.1016/j.ijhydene.2019.04.068, 2019.

Akagi, S. K., Yokelson, R. J., Wiedinmyer, C., Alvarado, M. J., Reid, J. S., Karl, T., Crounse, J. D., and Wennberg, P. O.: Emission factors for open and domestic biomass burning for use in atmospheric models, Atmos. Chem. Phys., 11, 4039–4072, https://doi.org/10.5194/acp-11-4039-2011, 2011.

American Academy of Microbiology: Microbes in Models: Integrating Microbes into Earth System Models for Understanding Climate Change: Report on an American Academy of Microbiology Virtual Colloquium held on Dec. 6 and 8, 2022 Washington (DC), 2023.

Andreae, M. O.: Emission of trace gases and aerosols from biomass burning – an updated assessment, Atmospheric Chemistry and Physics, 19, 8523–8546, https://doi.org/10.5194/acp-19-8523-2019, 2019.

Arthur, D. and Vassilvitskii, S.: K-means++: The advantages of careful seeding, Proceedings of the eighteenth annual ACM-SIAM symposium on discreate algorithm, 2007.

Bay, S. K., Dong, X., Bradley, J. A., Leung, P. M., Grinter, R., Jirapanjawat, T., Arndt, S. K., Cook, P. L. M., LaRowe, D. E., Nauer, P. A., Chiri, E., and Greening, C.: Trace gas oxidizers are widespread and active members of soil microbial communities, Nature Microbiology, 6, 246–256, https://doi.org/10.1038/s41564-020-00811-w, 2021.

Bertagni, M. B., Paulot, F., and Porporato, A.: Moisture Fluctuations Modulate Abiotic and Biotic Limitations of H_2 Soil Uptake, Global Biogeochemical Cycles, 35, https://doi.org/10.1029/2021gb006987, 2021.

Bertagni, M. B., Pacala, S. W., Paulot, F., and Porporato, A.: Risk of the hydrogen economy for atmospheric methane, Nature Communications, 13, https://doi.org/10.1038/s41467-022-35419-7, 2022.

Constant, P., Poissant, L., and Villemur, R.: Isolation of Streptomyces sp. PCB7, the first microorganism demonstrating high-affinity uptake of tropospheric H_2, The ISME Journal, 2, 1066–1076, https://doi.org/10.1038/ismej.2008.59, 2008.

da Silva Veras, T., Mozer, T. S., da Costa Rubim Messeder dos Santos, D., and da Silva César, A.: Hydrogen: Trends, production and characterization of the main process worldwide, International Journal of Hydrogen Energy, 42, 2018–2033, https://doi.org/10.1016/j.ijhydene.2016.08.219, 2017.

Dawood, F., Anda, M., and Shafiullah, G.: Hydrogen production for energy: An overview, International Journal of Hydrogen Energy, 45, 3847–3869, https://doi.org/10.1016/j.ijhydene.2019.12.059, 2020.

Derwent, R. G., Collins, W. J., Johnson, C. E., and Stevenson, D. S.: Transient Behaviour of Tropospheric Ozone Precursors in a Global 3-D CTM and Their Indirect Greenhouse Effects, Climatic Change, 49, 463–487, https://doi.org/10.1023/a:1010648913655, 2001.

Derwent, R. G., Simmonds, P. G., Doherty, S. J. O., Spain, T. G., and Young, D.: Natural greenhouse gas and ozone-depleting substance sources and sinks from the peat bogs of Connemara, Ireland from 1994–2020, Environmental Science: Atmospheres, 1, 406–415, https://doi.org/10.1039/d1ea00040c, 2021.

Derwent, R. G., Simmonds, P. G., O'Doherty, S., Manning, A. J., and Spain, T. G.: High-frequency, continuous hydrogen observations at Mace Head, Ireland from 1994 to 2022: Baselines, pollution events and 'missing' sources, Atmospheric Environment, 312, 120 029, https://doi.org/10.1016/j.atmosenv.2023.120029, 2023.

Dunne, J. P., Horowitz, L. W., Adcroft, A. J., Ginoux, P., Held, I. M., John, J. G., Krasting, J. P., Malyshev, S., Naik, V., Paulot, F., Shevliakova, E., Stock, C. A., Zadeh, N., Balaji, V., Blanton, C., Dunne, K. A., Dupuis, C., Durachta, J., Dussin, R., Gauthier, P. P. G., Griffies, S. M., Guo, H., Hallberg, R. W., Harrison, M., He, J., Hurlin, W., McHugh, C., Menzel, R., Milly, P. C. D., Nikonov, S., Paynter, D. J., Ploshay, J.,

Radhakrishnan, A., Rand, K., Reichl, B. G., Robinson, T., Schwarzkopf, D. M., Sentman, L. T., Underwood, S., Vahlenkamp, H., Winton, M., Wittenberg, A. T., Wyman, B., Zeng, Y., and Zhao, M.: The GFDL Earth System Model version 4.1 (GFDL-ESM 4.1): Overall coupled model description and simulation characteristics, Journal of Advances in Modeling Earth Systems, https://doi.org/10.1029/2019ms002015, 2020.

Ehhalt, D. and Rohrer, F.: Deposition velocity of H_2: a new algorithm for its dependence on soil moisture and temperature, Tellus B: Chemical and Physical Meteorology, 65, 19 904, https://doi.org/10.3402/tellusb.v65i0.19904, 2013.

Ehhalt, D. H. and Rohrer, F.: The tropospheric cycle of H_2: a critical review, Tellus B: Chemical and Physical Meteorology, 61, 500–535, https://doi.org/10.1111/j.1600-0889.2009.00416.x, 2009.

Francey, R. J., Steele, L. P., Spencer, D. A., Langenfelds, R. L., Law, R. M., Krummel, P. B., Fraser, P. J., Etheridge, D. M., Derek, N., Coram, S. A., Cooper, L. N., Allison, C. E., Porter, L., and Baly, S.: The CSIRO (Australia) measurement of greenhouse gases in the global atmosphere., Tech. rep., http://hdl.handle.net/102.100.100/191835?index=1, 2003.

Ghosh, A., Patra, P. K., Ishijima, K., Umezawa, T., Ito, A., Etheridge, D. M., Sugawara, S., Kawamura, K., Miller, J. B., Dlugokencky, E. J., Krummel, P. B., Fraser, P. J., Steele, L. P., Langenfelds, R. L., Trudinger, C. M., White, J. W. C., Vaughn, B., Saeki, T., Aoki, S., and Nakazawa, T.: Variations in global methane sources and sinks during 1910–2010, Atmospheric Chemistry and Physics, 15, 2595–2612, https://doi.org/10.5194/acp-15-2595-2015, 2015.

Global Monitoring Laboratory: Carbon Cycle Gases observation sites, https://www.gml.noaa.gov/dv/site/?program=ccgg, 2023.

Granier, C., Lamarque, J. F., Mieville, A., Müller, J. F., Olivier, J., Orlando, J., Peters, J., Petron, G., Tyndall, G., and Wallens, S.: POET, a database of surface emissions of ozone precursors, available on internet at http://www.aero.jussieu.fr/projet/ACCENT/POET.php, Tech. rep., 2005.

Grant, A., Archibald, A. T., Cooke, M. C., Nickless, G., and Shallcross, D. E.: Modelling the oxidation of 15 VOCs to track yields of hydrogen, Atmospheric Science Letters, 11, 265–269, https://doi.org/10.1002/asl.286, 2010.

Greening, C. and Grinter, R.: Microbial oxidation of atmospheric trace gases, Nature Reviews Microbiology, 20, 513–528, https://doi.org/10.1038/s41579-022-00724-x, 2022.

Greening, C., Constant, P., Hards, K., Morales, S. E., Oakeshott, J. G., Russell, R. J., Taylor, M. C., Berney, M., Conrad, R., and Cook, G. M.: Atmospheric Hydrogen Scavenging: from Enzymes to Ecosystems, Applied and Environmental Microbiology, 81, 1190–1199, https://doi.org/10.1128/aem.03364-14, 2015.

Guenther, A. B., Jiang, X., Heald, C. L., Sakulyanontvittaya, T., Duhl, T., Emmons, L. K., and Wang, X.: The Model of Emissions of Gases and Aerosols from Nature version 2.1 (MEGAN2.1): an extended and updated framework for modeling biogenic emissions, Geoscientific Model Development, 5, 1471–1492, https://doi.org/10.5194/gmd-5-1471-2012, 2012.

Hauglustaine, D., Paulot, F., Collins, W., Derwent, R., Sand, M., and Boucher, O.: Climate benefit of a future hydrogen economy, Communications Earth & Environment, 3, https://doi.org/10.1038/s43247-022-00626-z, 2022.

Holladay, J., Hu, J., King, D., and Wang, Y.: An overview of hydrogen production technologies, Catalysis Today, 139, 244–260, https://doi.org/10.1016/j.cattod.2008.08.039, 2009.

Horowitz, L. W., Naik, V., Paulot, F., Ginoux, P. A., Dunne, J. P., Mao, J., Schnell, J., Chen, X., He, J., John, J. G., Lin, M., Lin, P., Malyshev, S., Paynter, D., Shevliakova, E., and Zhao, M.: The GFDL Global Atmospheric Chemistry-Climate Model AM4.1: Model Description and Simulation Characteristics, Journal of Advances in Modeling Earth Systems, https://doi.org/10.1029/2019ms002032, 2020.

Howarth, R. W. and Jacobson, M. Z.: How green is blue hydrogen?, Energy Science & Engineering, 9, 1676–1687, https://doi.org/10.1002/ese3.956, 2021.

Huang, J., Yu, H., Guan, X., Wang, G., and Guo, R.: Accelerated dryland expansion under climate change, Nature Climate Change, 6, 166–171, https://doi.org/10.1038/nclimate2837, 2015.

Hydrogen Council: Hydrogen scaling up. A sustainable pathway for the global energy transition, 2017.

International Energy Agency: The Future of Hydrogen – Seizing today's opportunities, Tech. rep., International Energy Agency, Paris, France, 2019.

International Energy Agency: Global Hydrogen Review 2022, Tech. rep., International Energy Agency, Paris, France, 2022.

Jansson, J. K. and Hofmockel, K. S.: Soil microbiomes and climate change, Nature Reviews Microbiology, 18, 35–46, https://doi.org/10.1038/s41579-019-0265-7, 2019.

Jordaan, K., Lappan, R., Dong, X., Aitkenhead, I. J., Bay, S. K., Chiri, E., Wieler, N., Meredith, L. K., Cowan, D. A., Chown, S. L., and Greening, C.: Hydrogen-Oxidizing Bacteria Are Abundant in Desert Soils and Strongly Stimulated by Hydration, mSystems, 5, https://doi.org/10.1128/msystems.01131-20, 2020.

Jordan, A. and Steinberg, B.: Calibration of atmospheric hydrogen measurements, Atmospheric Measurement Techniques, 4, 509–521, https://doi.org/10.5194/amt-4-509-2011, 2011.

Kalnay, E., Kanamitsu, M., Kistler, R., Collins, W., Deaven, D., Gandin, L., Iredell, M., Saha, S., White, G., Woollen, J., Zhu, Y., Leetmaa, A., Reynolds, R., Chelliah, M., Ebisuzaki, W., Higgins, W., Janowiak, J., Mo, K. C., Ropelewski, C., Wang, J., Jenne, R., and Joseph, D.: The NCEP/NCAR 40-Year Reanalysis Project, Bull. Am. Meteorol. Soc., 77, 437–471, 1996.

Khdhiri, M., Hesse, L., Popa, M. E., Quiza, L., Lalonde, I., Meredith, L. K., Röckmann, T., and Constant, P.: Soil carbon content and relative abundance of high affinity H_2-oxidizing bacteria predict atmospheric H_2 soil uptake activity better than soil microbial community composition, Soil Biology and Biochemistry, 85, 1–9, https://doi.org/10.1016/j.soilbio.2015.02.030, 2015.

Lapi, T., Chatzimpiros, P., Raineau, L., and Prinzhofer, A.: System approach to natural versus manufactured hydrogen: An interdisciplinary perspective on a new primary energy source, International Journal of Hydrogen Energy, 47, 21 701–21 712, https://doi.org/10.1016/j.ijhydene.2022.05.039, 2022.

Lefeuvre, N., Truche, L., Donzé, F., Ducoux, M., Barré, G., Fakoury, R., Calassou, S., and Gaucher, E. C.: Native H2 Exploration in the Western Pyrenean Foothills, Geochemistry, Geophysics, Geosystems, 22, https://doi.org/10.1029/2021gc009917, 2021.

Li, J., Mao, J., Min, K.-E., Washenfelder, R. A., Brown, S. S., Kaiser, J., Keutsch, F. N., Volkamer, R., Wolfe, G. M., Hanisco, T. F., Pollack, I. B., Ryerson, T. B., Graus, M., Gilman, J. B., Lerner, B. M., Warneke, C., de Gouw, J. A., Middlebrook, A. M., Liao, J., Welti, A., Henderson, B. H., McNeill, V. F., Hall, S. R., Ullmann, K., Donner, L. J., Paulot, F., and Horowitz, L. W.: Observational constraints on glyoxal production from isoprene oxidation and its contribution to organic aerosol over the Southeast United States, J. Geophys. Res. Atmos., 121, 9849–9861, https://doi.org/10.1002/2016JD025331, 2016JD025331, 2016.

Meinshausen, M., Vogel, E., Nauels, A., Lorbacher, K., Meinshausen, N., Etheridge, D. M., Fraser, P. J., Montzka, S. A., Rayner, P. J., Trudinger, C. M., Krummel, P. B., Beyerle, U., Canadell, J. G., Daniel, J. S., Enting, I. G., Law, R. M., Lunder, C. R., O'Doherty, S., Prinn, R. G., Reimann, S., Rubino, M., Velders, G. J. M., Vollmer, M. K., Wang, R. H. J., and Weiss, R.: Historical greenhouse gas concentrations for climate modelling (CMIP6), Geoscientific Model Development, 10, 2057–2116, https://doi.org/10.5194/gmd-10-2057-2017, 2017.

Meinshausen, M., Nicholls, Z. R. J., Lewis, J., Gidden, M. J., Vogel, E., Freund, M., Beyerle, U., Gessner, C., Nauels, A., Bauer, N., Canadell, J. G., Daniel, J. S., John, A., Krummel, P. B., Luderer, G., Meinshausen, N., Montzka, S. A., Rayner, P. J., Reimann, S., Smith, S. J., van den Berg, M., Velders, G. J. M., Vollmer, M. K., and Wang, R. H. J.: The shared socio-economic pathway (SSP) greenhouse gas concentrations and their extensions to 2500, Geoscientific Model Development, 13, 3571–3605, https://doi.org/10.5194/gmd-13-3571-2020, 2020.

Meredith, L. K., Commane, R., Keenan, T. F., Klosterman, S. T., Munger, J. W., Templer, P. H., Tang, J., Wofsy, S. C., and Prinn, R. G.: Ecosystem fluxes of hydrogen in a mid-latitude forest driven by soil microorganisms and plants, Global Change Biology, 23, 906–919, https://doi.org/10.1111/gcb.13463, 2016.

Milkov, A. V.: Molecular hydrogen in surface and subsurface natural gases: Abundance, origins and ideas for deliberate exploration, Earth-Science Reviews, 230, 104 063, https://doi.org/10.1016/j.earscirev.2022.104063, 2022.

Ocko, I. B. and Hamburg, S. P.: Climate consequences of hydrogen emissions, Atmospheric Chemistry and Physics, 22, 9349–9368, https://doi.org/10.5194/acp-22-9349-2022, 2022.

O'Rourke, P., Smith, S., Mott, A., Ahsan, H., Mcduffie, E., Crippa, M., Klimont, Z., Mcdonald, B., Wang, S., Nicholson, M., Hoesly, R., and Feng, L.: CEDS v_2021_04_21 Gridded emissions data, https://doi.org/10.25584/PNNLDATAHUB/1779095, 2021.

Paulot, F., Paynter, D., Naik, V., Malyshev, S., Menzel, R., and Horowitz, L. W.: Global modeling of hydrogen using GFDL-AM4.1: Sensitivity of soil removal and radiative forcing, International Journal of Hydrogen Energy, 46, 13 446–13 460, https://doi.org/10.1016/j.ijhydene.2021.01.088, 2021.

Pétron, G., Crotwell, A., Crotwell, M., Kitzis, D., Madronich, M., Mefford, T., Moglia, E., Mund, J., Neff, D., Thoning, K., and Wolter, S.: Atmospheric Hydrogen Dry Air Mole Fractions from the NOAA GML Carbon Cycle Cooperative Global Air Sampling Network, 2009-Present, https://doi.org/10.15138/WP0W-EZ08, 2023.

Pétron, G., Crotwell, A., Mund, J., Crotwell, M., Mefford, T., Thoning, K., Hall, B., Kitzis, D., Madronich, M., Moglia, E., Neff, D., Wolter, S., Jordan, A., Krummel, P., Langenfeld, R., Patterson, J. D., and Andrews, A.: Atmospheric H_2 observations from the NOAA Global Greenhouse Gas Reference Network, Atmospheric Measurement Techniques Discussion [preprint], https://doi.org/10.5194/amt-2024-4, in review, 2024.

Price, H., Jaeglé, L., Rice, A., Quay, P., Novelli, P. C., and Gammon, R.: Global budget of molecular hydrogen and its deuterium content: Constraints from ground station, cruise, and aircraft observations, Journal of Geophysical Research, 112, https://doi.org/10.1029/2006jd008152, 2007.

Prinn, R. G., Weiss, R. F., Arduini, J., Arnold, T., DeWitt, H. L., Fraser, P. J., Ganesan, A. L., Gasore, J., Harth, C. M., Hermansen, O., and et al.: History of chemically and radiatively important atmospheric gases from the Advanced Global Atmospheric Gases Experiment (AGAGE), Earth System Science Data, 10, 985–1018, https://doi.org/10.5194/essd-10-985-2018, 2018.

Prinzhofer, A., Cissé, C. S. T., and Diallo, A. B.: Discovery of a large accumulation of natural hydrogen in Bourakebougou (Mali), International Journal of Hydrogen Energy, 43, 19 315–19 326, https://doi.org/10.1016/j.ijhydene.2018.08.193, 2018.

Rayner, N. A., Parker, D. E., Horton, E. B., Folland, C. K., Alexander, L. V., Rowell, D. P., Kent, E. C., and Kaplan, A.: Global analyses of sea surface temperature, sea ice, and night marine air temperature since the late nineteenth century, J. Geophys. Res. Atmos., 108, 4407, https://doi.org/10.1029/2002JD002670, 2003.

Rodell, M., Houser, P. R., Jambor, U., Gottschalck, J., Mitchell, K., Meng, C.-J., Arsenault, K., Cosgrove, B., Radakovich, J., Bosilovich, M., Entin, J. K., Walker, J. P., Lohmann, D., and Toll, D.: The Global Land Data Assimilation System, Bulletin of the American Meteorological Society, 85, 381–394, https://doi.org/10.1175/bams-85-3-381, 2004.

Röth, E.-P. and Ehhalt, D. H.: A simple formulation of the CH_2O photolysis quantum yields, Atmospheric Chemistry and Physics, 15, 7195–7202, https://doi.org/10.5194/acp-15-7195-2015, 2015.

Sand, M., Skeie, R. B., Sandstad, M., Krishnan, S., Myhre, G., Bryant, H., Derwent, R., Hauglustaine, D., Paulot, F., Prather, M., and Stevenson, D.: A multi-model assessment of the Global Warming Potential of hydrogen, Communications Earth & Environment, 4, https://doi.org/10.1038/s43247-023-00857-8, 2023.

Saunois, M., Stavert, A. R., Poulter, B., Bousquet, P., Canadell, J. G., Jackson, R. B., Raymond, P. A., Dlugokencky, E. J., Houweling, S., Patra, P. K., Ciais, P., Arora, V. K., Bastviken, D., Bergamaschi, P., Blake, D. R., Brailsford, G., Bruhwiler, L., Carlson, K. M., Carrol, M., Castaldi, S., Chandra, N., Crevoisier, C., Crill, P. M., Covey, K., Curry, C. L., Etiope, G., Frankenberg, C., Gedney, N., Hegglin, M. I., Höglund-Isaksson, L., Hugelius, G., Ishizawa, M., Ito, A., Janssens-Maenhout, G., Jensen, K. M., Joos, F., Kleinen, T., Krummel, P. B., Langenfelds, R. L., Laruelle, G. G., Liu, L., Machida, T., Maksyutov, S., McDonald, K. C., McNorton, J., Miller, P. A., Melton, J. R., Morino, I., Müller, J., Murguia-Flores, F., Naik, V., Niwa, Y., Noce, S., O'Doherty, S., Parker, R. J., Peng, C., Peng, S., Peters, G. P., Prigent, C., Prinn, R., Ramonet, M., Regnier, P., Riley, W. J., Rosentreter, J. A., Segers, A., Simpson, I. J., Shi, H., Smith, S. J., Steele, L. P., Thornton, B. F., Tian, H., Tohjima, Y., Tubiello, F. N., Tsuruta, A., Viovy, N., Voulgarakis, A., Weber, T. S., van Weele, M., van der Werf, G. R., Weiss, R. F., Worthy, D., Wunch, D., Yin, Y., Yoshida, Y., Zhang, W., Zhang, Z., Zhao, Y., Zheng, B., Zhu, Q., Zhu, Q., and Zhuang, Q.: The Global Methane Budget 2000–2017, Earth System Science Data, 12, 1561–1623, https://doi.org/10.5194/essd-12-1561-2020, 2020.

Smith-Downey, N. V., Randerson, J. T., and Eiler, J. M.: Temperature and moisture dependence of soil H_2 uptake measured in the laboratory, Geophysical Research Letters, 33, https://doi.org/10.1029/2006gl026749, 2006.

Smith-Downey, N. V., Randerson, J. T., and Eiler, J. M.: Molecular hydrogen uptake by soils in forest, desert, and marsh ecosystems in California, Journal of Geophysical Research, 113, https://doi.org/10.1029/2008jg000701, 2008.

Staffell, I., Scamman, D., Abad, A. V., Balcombe, P., Dodds, P. E., Ekins, P., Shah, N., and Ward, K. R.: The role of hydrogen and fuel cells in the global energy system, Energy & Environmental Science, 12, 463–491, https://doi.org/10.1039/c8ee01157e, 2019.

Taylor, K. E., Williamson, D., and Zwiers, F.: The sea surface temperature and sea-ice concentration boundary conditions for AMIP II simulations, Program for Climate Model Diagnosis and Intercomparison, Lawrence Livermore National Laboratory, University of California, 2000.

van der Werf, G. R., Randerson, J. T., Giglio, L., Collatz, G. J., Kasibhatla, P. S., and Arellano, A. F.: Interannual variability in global biomass burning emissions from 1997 to 2004, Atmospheric Chemistry and Physics, 6, 3423–3441, https://doi.org/10.5194/acp-6-3423-2006, 2006.

van der Werf, G. R., Randerson, J. T., Giglio, L., van Leeuwen, T. T., Chen, Y., Roğers, B. M., Mu, M., van Marle, M. J. E., Morton, D. C., Collatz, G. J., Yokelson, R. J., and Ǩasibhatla, P. S.: Global fire emissions estimates during 1997–2016, Earth System Science Data, 9, 697–720, https://doi.org/10.5194/essd-9-697-2017, 2017.

WMO: WMO Greenhouse Gas Bulletin, Tech. Rep. 17, Japan Meterological Agency and WMO, 2021.

Yashiro, H., Sudo, K., Yonemura, S., and Takigawa, M.: The impact of soil uptake on the global distribution of molecular hydrogen: chemical transport model simulation, Atmospheric Chemistry and Physics, 11, 6701–6719, https://doi.org/10.5194/acp-11-6701-2011, 2011.

Zgonnik, V.: The occurrence and geoscience of natural hydrogen: A comprehensive review, Earth-Science Reviews, 203, 103 140, https://doi.org/10.1016/j.earscirev.2020.103140, 2020.